**Lensa: Jurnal Kependidikan Fisika**
Penerbit: Universitas Pendidikan Mandalika
https://e-journal.undikma.ac.id/index.php/Lensa/index

Dec. 2026, Vol. 14, No. 2
e-ISSN: 2686-0937
pp. 235–244

# Directional Photon-Statistics Contrast in a Two-Emitter Chiral Waveguide Quantum Electrodynamics

**I Gusti Ngurah Yudi Handayana[1]*, Siti Alaa[1,2], Lily Maysari Angraini[1], Ramadian Ridho Illahi[1], Marzuki[1], I Wayan Sudiarta[1]**

[1] Department of Physics, University of Mataram, Mataram, Indonesia
[2] Discipline of Chemical Engineering, WA School of Mines, Curtin University, Bentley, Australia

**Corresponding Author: ngurahyudi@unram.ac.id*

## Abstract

The propagation direction of light emitted from coupled quantum emitters need not determine its photon-counting statistics. Here we examine steady-state intensity and second-order photon correlations from two uniformly side-driven two-level emitters coupled to a linear chiral waveguide. A Lindblad master equation with direction-resolved collective emission operators is solved without restricting the emitter excitation number. At a driving strength of $\Omega = 0.3\gamma$, zero detuning, chirality $D = 0.5$, and propagation phase $\varphi = \pi/4$, the normalized right- and left-going photon fluxes are 0.046591 and 0.041187, respectively. Despite the small intensity directionality of approximately 0.062, the zero-delay correlations differ markedly: $g_R^{(2)}(0) = 2.589$ indicates bunching, whereas $g_L^{(2)}(0) = 0.368$ indicates antibunching. Parameter maps over 77 chirality values and 79 propagation phases reveal several separated regions in which the emission intensities remain nearly balanced while the photon statistics exhibit opposite behavior. This contrast is understood from collective interference, which suppresses the stronger-coupled output and enhances the weaker-coupled output, whereas two-photon coincidences retain different directional coupling factors. The results identify a compact operating regime for direction-selective photon statistics in a minimal driven waveguide-QED system.

**Keywords:** Chiral WQED; Collective interference; Directional emission; Photon antibunching; Photon correlations

**How to cite:** Handayana, I. G. N. Y., Alaa, S., Angraini, L. M., Illahi, R. R., Marzuki, M., & Sudiarta, I. W. (2026). Directional Photon-Statistics Contrast in a Two-Emitter Chiral Waveguide Quantum Electrodynamics. *Lensa: Jurnal Kependidikan Fisika*, *14*(2), 235–244. https://doi.org/10.33394/j-lkf.v14i2.23215

## INTRODUCTION

Waveguide quantum electrodynamics (WQED) provides a platform for studying light–matter interactions in which spatially separated quantum emitters are coupled through guided electromagnetic modes. Unlike free-space systems, the confinement of light in a one-dimensional waveguide allows photon-mediated interactions to extend over relatively long distances, giving rise to collective emission and coherent excitation exchange among emitters (Sheremet et al., 2023). An important feature of WQED is the possibility of chiral light–matter coupling, where the interaction strength depends on the direction of photon propagation. Such directional coupling can arise from spin–momentum locking of guided light and the polarization-dependent transitions of quantum emitters, leading to asymmetric emission rates and nonreciprocal optical responses (Lodahl et al., 2017; Mahmoodian et al., 2016; Sheremet et al., 2023). Advances in nanophotonic structures have further enabled control over directional emission through the

engineering of emitter polarization and waveguide geometry (Hallett et al., 2022; Rosiński et al., 2024).

The presence of chirality can substantially modify the collective behavior of quantum emitters, influencing excitation transport, interference between emission pathways, and the properties of the emitted light (Söllner et al., 2015). While directional emission is commonly characterized by comparing the photon intensities propagating to the right and left, the mean intensity alone does not provide a complete description of the output field. Photon correlations offer additional information about the statistical properties of the emitted light, particularly the tendency of photons to be detected close together or separated in time. These properties are commonly characterized by the second-order intensity correlation function, which distinguishes photon antibunching from bunching. Previous studies have explored photon correlations and nonlinear optical responses in waveguide-coupled systems, including correlated few-photon transport, two-photon scattering, and the control of photon statistics (Crowder et al., 2022; Gu et al., 2024; Le Jeannic et al., 2021; Mahmoodian et al., 2018).

The control of photon emission in WQED is closely related to the interplay between collective interactions, propagation phases, and the directional coupling of quantum emitters to the guided modes. Interference between different emission pathways can enhance or suppress collective radiation, while the asymmetry of the coupling provides an additional means of controlling the direction of photon emission (Pennetta, Blaha, et al., 2022; Pennetta, Lechner, et al., 2022) . Theoretical studies have shown how these mechanisms lead to directional collective decay and tunable radiative behavior in waveguide-coupled emitters (Solano et al., 2023; Yao & Li, 2025). Beyond the mean emission properties, chirality can also modify the quantum statistics of the output field. In particular, nonreciprocal transmission and reflection can exhibit distinct photon correlations, including regimes of nonclassical light characterized by photon antibunching (Miao & Agarwal, 2025). These findings highlight the role of directional coupling not only in controlling photon emission but also in shaping its statistical properties.

Experimental progress has established several platforms for investigating chiral light–matter interactions, including atoms coupled to optical nanofibers, quantum dots embedded in photonic crystal waveguides, and superconducting artificial atoms coupled to microwave waveguides (Javadi et al., 2015; Joshi et al., 2023; Mitsch et al., 2014; Söllner et al., 2015). These systems offer different approaches to controlling directional emission through emitter polarization, engineered optical modes, and interference between coupling pathways. More recently, Chirality-dependent photon correlations have been demonstrated in electrically tunable quantum-dot dimers (Hallacy et al., 2026) . Directional photon statistics from two radiatively coupled quantum dots in a bidirectional waveguide also has been reported where single-photon and photon-pair emission could be selectively observed at opposite output ports (Hansen et al., 2026; Henke et al., 2026; Hotter et al., 2026). These experimental developments demonstrate the growing ability to control both the direction and statistical properties of emitted photons, motivating further investigation of the relationship between photon intensity and photon correlations in waveguide-coupled systems.

In this work, we investigate two identical two-level emitters coupled to a linear chiral waveguide and driven coherently from the side. We map the steady-state guided intensities and zero-delay second-order correlations over the chirality and interemitter propagation phase. We then identify nearly intensity-balanced operating regions and trace the observed contrast to interference between the two indistinguishable emitter-to-port pathways. The analysis is deliberately restricted to the ideal two-emitter configuration, allowing the relation between direction-dependent mean emission and photon statistics to be assessed.

## METHODS

### Two-emitter chiral waveguide model

In our model, two identical two-level emitters are positioned at $x_1 = 0$ and $x_2 = d$ along a one-dimensional waveguide. The atomic lowering and raising operators are denoted by $\sigma_j = |g\rangle_j\langle e|$ and $\sigma_j^\dagger$, respectively. The model follows the Markovian chiral spin-network framework (Pichler et al., 2015), with negligible nonguided decay and identical in-phase coherent driving from a transverse field. In units with $\hbar = 1$, the reduced atomic density matrix obeys the Lindblad master equation

$$\frac{d\rho}{dt} = -i[H,\rho] + \sum_{\alpha=R,L} \mathcal{D}[J_\alpha]\rho, \quad \mathcal{D}[J]\rho = J\rho J^\dagger - \frac{1}{2}\{J^\dagger J, \rho\}. \tag{1}$$

Here the coherent dynamics contains the transverse driving, detuning, and direction-dependent waveguide-mediated exchange contributions:

$$H = H_{\text{drive}} + H_{\text{det}} + H_R + H_L. \tag{2}$$

$$H_{\text{drive}} = \frac{\Omega}{2}\sum_{j=1}^{2}(\sigma_j^\dagger + \sigma_j), \quad H_{\text{det}} = -\Delta\sum_{j=1}^{2}\sigma_j^\dagger\sigma_j. \tag{3}$$

The detuning is defined as $\Delta = \omega_d - \omega_0$, where $\omega_d$ and $\omega_0$ are the driving and atomic transition frequencies. The factor $\Omega/2$ specifies the Rabi-frequency. For emitters ordered from left to right, the coherent guided interactions are

$$H_R = -\frac{i\gamma_R}{2}(A_R - A_R^\dagger), \qquad H_L = -\frac{i\gamma_L}{2}(A_L - A_L^\dagger), \tag{4}$$

$$A_R = e^{i\phi}\sigma_2^\dagger\sigma_1, \qquad A_L = e^{i\phi}\sigma_1^\dagger\sigma_2. \tag{5}$$

The two directional decay rates and the propagation phase are parameterized by

$$\gamma_R = \frac{\gamma}{2}(1+D), \quad \gamma_L = \frac{\gamma}{2}(1-D), \quad \phi = kd. \tag{6}$$

The chirality parameter D varies from −1 to 1; $D = 0$ corresponds to equal directional coupling. For the right-going (R) and left-going (L) emitted fields, the collective jump operators are

$$J_R = \sqrt{\gamma_R}(\sigma_1 + e^{-i\phi}\sigma_2), \quad J_L = \sqrt{\gamma_L}(\sigma_1 + e^{i\phi}\sigma_2). \tag{7}$$

These operators coherently add the two indistinguishable atomic emission amplitudes reaching the same output port. They also generate the direction-resolved Lindblad dissipators in Eq. (1). The transverse drive is not injected through

a guided input port, so the observables below refer to emitted guided light, without an added coherent input-field background.

### Steady-state photon observables

For clarity, we adopt the ordered atomic basis $\{|m\rangle\} = \{|1\rangle, |2\rangle, |3\rangle, |4\rangle\} = \{|gg\rangle, |eg\rangle, |ge\rangle, |ee\rangle\}$, with state populations $P_{\mathrm{m}} = \langle m|\rho_{ss}|m\rangle$. The mean excitation number and the simultaneous two-emitter excitation probability are

$$\langle N_{\mathrm{exc}}\rangle = P_2 + P_3 + 2P_4, \quad P_4 = \langle n_1 n_2\rangle, \quad n_j = \sigma_j^{\dagger}\sigma_j. \tag{8}$$

The steady-state emitted photon flux in output channel $\alpha \in \{R, L\}$ is

$$I_\alpha = \mathrm{Tr}\left(J_\alpha^{\dagger} J_\alpha \rho_{\mathrm{ss}}\right). \tag{9}$$

Photon statistics are characterized by the normally ordered, zero-delay second-order correlation,

$$g_\alpha^{(2)}(0) = \frac{\mathrm{Tr}\left[\left(J_\alpha^{\dagger}\right)^2 J_\alpha^2 \rho_{\mathrm{ss}}\right]}{I_\alpha^2} = \frac{G_\alpha^{(2)}(0)}{I_\alpha^2}. \tag{10}$$

A value $g_\alpha{}^{(2)}(0) < 1$ indicates suppression of near-simultaneous detections, while $g_\alpha{}^{(2)}(0) > 1$ indicates bunching relative to independent photon arrivals. The corresponding temporal correlation is evaluated by quantum regression as

$$g_\alpha^{(2)}(\tau) = \frac{\mathrm{Tr}\left[J_\alpha^{\dagger} J_\alpha e^{\mathcal{L}\tau}\left(J_\alpha \rho_{\mathrm{ss}} J_\alpha^{\dagger}\right)\right]}{I_\alpha^2}. \tag{11}$$

The two directional contrasts considered here are the normalized intensity asymmetry and the difference between zero-delay correlations:

$$\mathcal{D}_I = \frac{I_R - I_L}{I_R + I_L}, \qquad \Delta g^{(2)} = g_R^{(2)}(0) - g_L^{(2)}(0). \tag{12}$$

For each $(D, \varphi)$ pair, the complete four-dimensional two-emitter Hilbert space is retained and the stationary state is obtained from the full 16 × 16 Liouvillian with a trace constraint. The calculations employ QuantumOptics.jl and double-precision linear algebra (Krämer et al., 2018). The guided decay scale is set to $\gamma = 1$, with $\Omega = 0.3\gamma$ and $\Delta = 0$. The parameter grid contains 77 equally spaced chirality values, $D = -0.95, -0.925, \ldots, 0.95$, and 79 phases from $0.025\pi$ to $1.975\pi$ in steps of $0.025\pi$, giving 6,083 configurations. The exact endpoints $\varphi = 0$ and $2\pi$ are excluded to avoid a nonunique stationary sector at $D = 0$. For the temporal benchmark, $\gamma\tau$ ranges from 0 to 30 at 301 points.

The normalized $g^{(2)}$ maps are masked wherever the corresponding photon flux is below $I_{cut} = max(10^{-8}\gamma, 10^{-3} I_{peak})$, with $I_{peak}$ the largest directional intensity over the grid. Raw fluxes and correlation numerators are retained without masking. The plotted colors of $g^{(2)}$ are saturated at 6 (and those of $\Delta g^{(2)}$ at $\pm 6$) solely for readability; this does not clip the underlying numerical data. Numerical checks include the mirror relation under $D \to -D$, the positivity of the stationary density matrix, and the two-emitter counting identity given below.

## RESULTS AND DISCUSSION

### Directional bunching and antibunching at comparable intensities

We first examine a representative resonant configuration with $D = 0.5$ and $\varphi = \pi/4$. The resulting steady-state intensities are $I_R/\gamma = 0.046591$ and $I_L/\gamma =$

$0.041187$, yielding a normalized intensity asymmetry of $\mathcal{D}_I = 0.062$. Thus, although the right-going emitter–waveguide coupling is three times the left-going coupling ($\gamma_R/\gamma_L = 3$), the two detected photon fluxes differ by only about $6.2\%$ according to the normalized contrast defined in Eq. (12).

The photon statistics are strikingly different at the same parameter point. The zero-delay correlation is $g_R{}^{(2)}(0) = 2.589$ for the right-going output and $g_L{}^{(2)}(0) = 0.368$ for the left-going output. Therefore, the right-going field is bunched, whereas the left-going field exhibits antibunching at zero delay. The ratio $g_R{}^{(2)}(0)/g_L{}^{(2)}(0)$ is approximately 7.03 even though their average photon fluxes are close. This contrast demonstrates why a directionality analysis based only on mean intensity can overlook major differences in photon detection statistics.

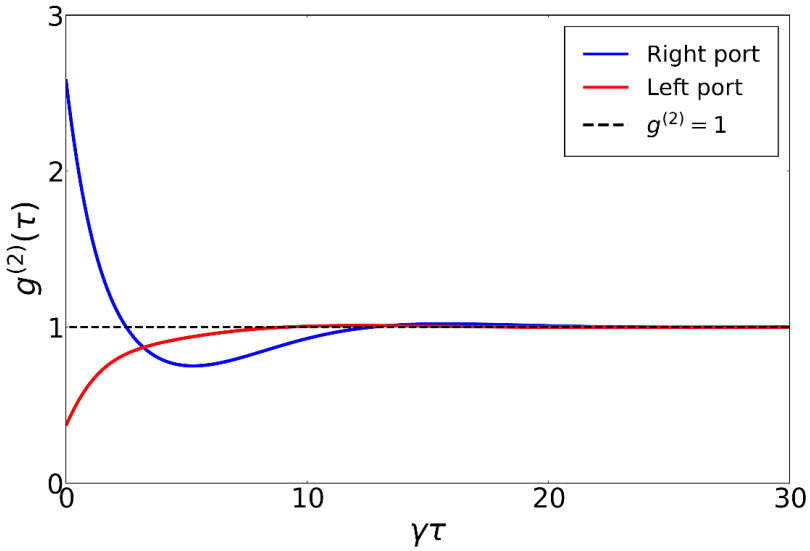


**Figure 1.** Steady-state second-order photon correlations for the right- and left-propagating emitted fields as functions of the scaled delay $\gamma\tau$ at $D = 0.5$, $\varphi = \pi/4$, $\Omega = 0.3\gamma$, and $\Delta = 0$. The dashed reference denotes $g^{(2)} = 1$. The two output ports exhibit bunching and antibunching, respectively, at zero delay.

The two-time correlations in Figure 1 provide an independent temporal view of the same steady-state emission. The right-going correlation begins above the uncorrelated level, initially decreases below unity, and then relaxes with a small transient overshoot. The left-going correlation starts below unity and approaches the uncorrelated reference more directly. Both channels approach $g^{(2)}(\tau) \approx 1$ for large delays, as expected when conditional detection correlations decay. The temporal behavior supports the zero-delay classification but does not imply that bunching or antibunching is maintained at all delays.

## Intensity and photon-statistics maps

Figure 2 presents the steady-state directional intensities and photon correlations across the chirality–phase plane. Figures 2(a) and 2(b) show that the flux distributions are exchanged under reversal of the coupling asymmetry $D$. The largest right-going emission occurs near positive $D$ and $\varphi/\pi \approx 1$, whereas the corresponding left-going enhancement appears near negative $D$. Away from these high-flux regions, the two fields can still exhibit comparable emission rates. This

distinction between the strength of the directional coupling and the measured flux is central to the present analysis.

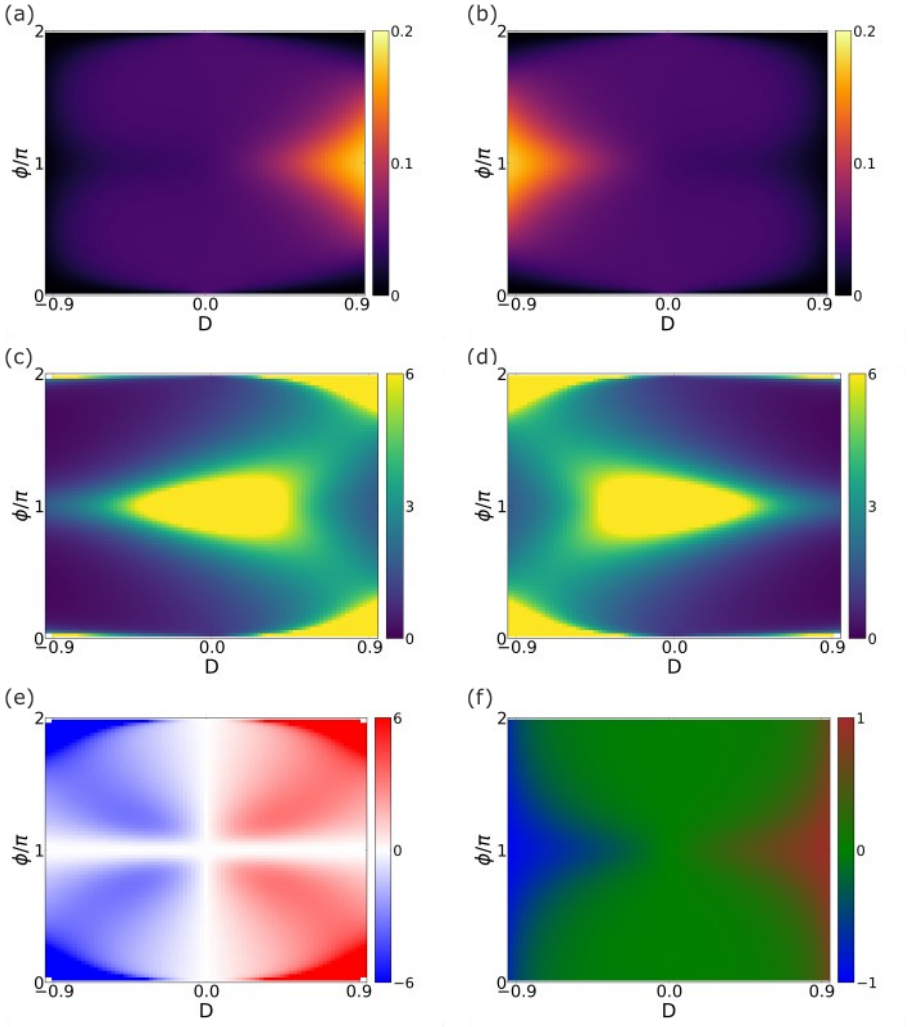


**Figure 2.** Direction-resolved steady-state photon emission mapped versus chirality D and propagation phase $\varphi/\pi$: (a) $I_R/\gamma$, (b) $I_L/\gamma$, (c) $g_R{}^{(2)}(0)$, (d) $g_L{}^{(2)}(0)$, (e) $\Delta g^{(2)}$, and (f) normalized intensity directionality $\mathcal{D}_I$. Parameters are $\Omega = 0.3\gamma$ and $\Delta = 0$.

Figures 2(c) and 2(d) reveal a different organization of the photon statistics. Extended, direction-exchanged regions exhibit normalized correlations above unity in one output and below unity in the other. The difference $\Delta g^{(2)}$, shown in Figure 2(e), changes sign when the chirality is reversed and vanishes on the reciprocal symmetry line $D = 0$. In contrast, Figure 2(f) shows that the intensity directionality $\mathcal{D}_I$ does not simply reproduce the spatial pattern of the normalized photon-statistical contrast. These parameter maps demonstrate that an intensity-based notion of directionality and a statistics-based one highlight different features of the same driven system.

## Nearly balanced operating regions and interference mechanism

To isolate a useful contrast from the trivial divergence of normalized correlations at vanishing photon flux, we identify parameter points that satisfy three simultaneous criteria: $|\mathcal{D}_I| \leq 0.10, g_R{}^{(2)}(0) \geq 2$ together with $g_L{}^{(2)}(0) \leq 0.5$, or the opposite assignment of the two ports, with both intensities above the common

masking threshold. Figure 3(a) highlights four separated regions associated with positive or negative chirality and reflection-related propagation phases. Their finite extent in parameter space shows that the selected behavior is not restricted to the single benchmark configuration, although its robustness outside the studied ideal model is not assessed here.

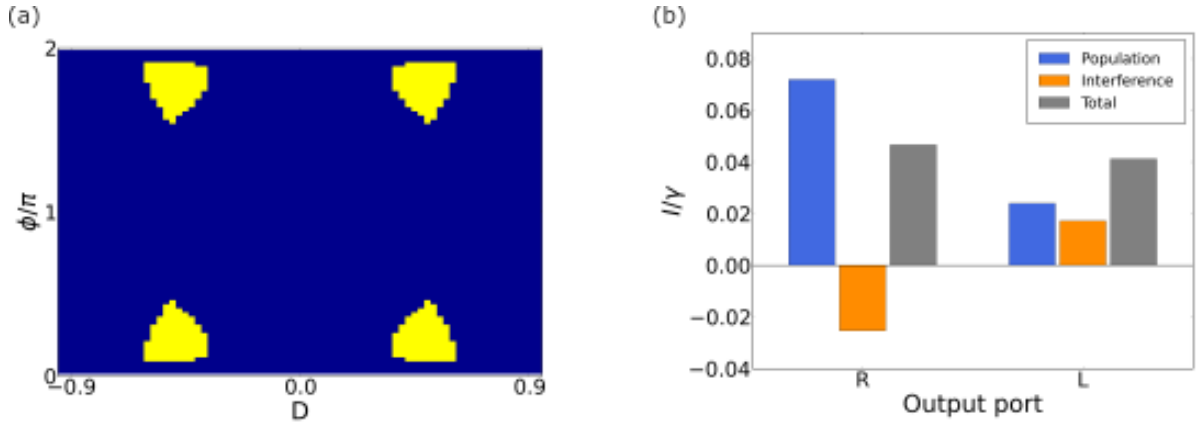


**Figure 3.** (a) Parameter regions with nearly balanced intensity ($|\mathcal{D}_I| \leq 0.10$) and opposite strong zero-delay statistics (one port $g^{(2)} \geq 2$ and the other $g^{(2)} \leq 0.5$), after applying the common intensity mask. (b) Population, interference, and total contributions to the directional output flux at $D = 0.5$ and $\varphi = \pi/4$. The contrast between the population and interference contributions explains the near balance of the detected intensities.

To understand why the intensities can remain comparable, let $C_{12} = \langle \sigma_1^{\dagger} \sigma_2 \rangle_{ss}$ denote the interemitter optical coherence. The directional intensity can be separated into an excitation-population contribution and a phase-sensitive collective-interference contribution:

$$I_R = \gamma_R \left[ \langle N_{\text{exc}} \rangle + 2\text{Re}\left( e^{-i\phi} C_{12} \right) \right], \tag{13}$$

$$I_L = \gamma_L \left[ \langle N_{\text{exc}} \rangle + 2\text{Re}\left( e^{i\phi} C_{12} \right) \right]. \tag{14}$$

At $D = 0.5$ and $\varphi = \pi/4$, the mean excitation number is $\langle N_{exc} \rangle = 0.095862$ and the coherence is $C_{12} = 0.012426 - 0.036284i$. The contributions $\gamma_R \langle N_{exc} \rangle / \gamma$ and $\gamma_L \langle N_{exc} \rangle / \gamma$ are approximately 0.071897 and 0.023966, respectively. Their difference is partially compensated by the interference contributions −0.025305 and +0.017222. As shown in Figure 3(b), the resulting total intensities become 0.046591 and 0.041187. The negative interference bar signifies destructive contribution to the output flux, not a negative physical photon rate.

The two-emitter Hilbert space also provides a compact relation for the unnormalized equal-time coincidence signals. Since $\sigma_j^2 = 0$ for each two-level emitter, the collective emission operators obey the identity

$$G_R^{(2)}(0) = 4\gamma_R^2 P_4, \qquad G_L^{(2)}(0) = 4\gamma_L^2 P_4. \tag{15}$$

Thus the coincidence numerators depend on the shared doubly excited population $P_4$ but carry different directional coupling factors. After normalization by the squared output intensities, the resulting correlations may be strongly unequal even

when the average fluxes are almost balanced. For two well-defined nonzero channel correlations, this is expressed by:

$$\frac{g_R^{(2)}(0)}{g_L^{(2)}(0)} = \left(\frac{\gamma_R}{\gamma_L}\right)^2 \left(\frac{I_L}{I_R}\right)^2. \quad (16)$$

The two observations are therefore linked: collective optical coherence modifies each measured intensity, while the zero-delay coincidence retains a simple dependence on $P_4$ and the directional decay rates. This is a quantitative explanation of the contrast rather than a claim that the two photon statistics can be independently adjusted. In particular, the ratio in Eq. (16) is fixed once the chirality and the two intensities are specified in the ideal two-emitter model.

## CONCLUSION

A driven pair of two-level emitters in a linear chiral waveguide can generate right- and left-propagating fields with almost equal average photon fluxes but markedly different second-order photon statistics. For $D = 0.5$ and $\varphi = \pi/4$, the intensity directionality is approximately 0.062, whereas the right-going field is bunched $[g_R{}^{(2)}(0) = 2.589]$ and the left-going field is antibunched $[g_L{}^{(2)}(0) = 0.368]$. A 6,083-point chirality–phase map reveals several separated parameter regions exhibiting the same qualitative contrast. The decomposition of the guided intensity shows that collective interference compensates the directional decay imbalance, while zero-delay coincidences retain their quadratic dependence on the output coupling rates and on the doubly excited-state population. These results provide a compact numerical characterization of directional photon-statistics contrast in an ideal two-emitter chiral waveguide and clarify why similar intensities do not imply similar counting statistics.

## RECOMMENDATION

Future work may assess the effects of unequal driving phases, emitter detuning, nonguided loss, and more than two emitters, where additional multiphoton interference pathways become available. Such extensions lie beyond the parameter range investigated in the present article.

## ACKNOWLEDGMENT

The authors would like to thank the IAMS Cluster for providing the computational resources used in this research

## REFERENCES

Crowder, G., Ramunno, L., & Hughes, S. (2022). Quantum trajectory theory and simulations of nonlinear spectra and multiphoton effects in waveguide-QED systems with a time-delayed coherent feedback. *Physical Review A*, *106*(1), Article 013714. https://doi.org/10.1103/PhysRevA.106.013714

Gu, W., Chen, L., Yi, Z., Liu, S., & Li, G. (2024). Tunable photon-photon correlations in waveguide QED systems with giant atoms. *Physical Review A*, *109*(2), Article 023720. https://doi.org/10.1103/PhysRevA.109.023720

Hallacy, L., Hallett, D., Fenzl, A., Martin, N. J., Dost, R., Verma, A., Fletcher, J., Farrer, I., Antwis, L., Skolnick, M. S., & Wilson, L. R. (2026). Chiral quantum optics with scalable quantum dot dimers. *npj Nanophotonics*, *3*(1), Article 40. https://doi.org/10.1038/s44310-026-00148-y

Hallett, D., Foster, A. P., Whittaker, D., Skolnick, M. S., & Wilson, L. R. (2022). Engineering chiral light-matter interactions in a waveguide-coupled nanocavity. *ACS Photonics*, *9*(2), 706–713. https://doi.org/10.1021/acsphotonics.1c01806

Hansen, L. M., Henke, C., Hotter, C., Sandberg, O. A. D., Sandø, T. W., Angelopoulou, V., Tiranov, A., Møller, C. B., Liu, Z., Midolo, L., Bart, N., Ludwig, A., Walther, P., van Diepen, C. J., Lodahl, P., & Sørensen, A. S. (2026). *Realization of waveguide many-body quantum optics* [Preprint]. arXiv. https://arxiv.org/abs/2605.18525

Henke, C., Sandø, T. W., Angelopoulou, V., Hansen, L. M., Tiranov, A., Sandberg, O. A. D., Liu, Z., Midolo, L., Bart, N., Ludwig, A., Sørensen, A. S., Lodahl, P., & van Diepen, C. J. (2026). Directional and correlated optical emission from a waveguide-engineered molecule with local control. *PRX Quantum*. https://doi.org/10.1103/v1r7-lr89

Hotter, C., Henke, C., van Diepen, C. J., Lodahl, P., & Søndberg Sørensen, A. (2026). Quantum non-Gaussianity criterion based on photon correlations g(2) and g(3). *Physical Review Letters*, *136*(24), Article 243601. https://doi.org/10.1103/1t2q-qm97

Javadi, A., Söllner, I., Arcari, M., Hansen, S. L., Midolo, L., Mahmoodian, S., Kiršansk-, G., Pregnolato, T., Lee, E. H., Song, J. D., Stobbe, S., & Lodahl, P. (2015). Single-photon non-linear optics with a quantum dot in a waveguide. *Nature Communications*, *6*, Article 8655. https://doi.org/10.1038/ncomms9655

Joshi, C., Yang, F., & Mirhosseini, M. (2023). Resonance fluorescence of a chiral artificial atom. *Physical Review X*, *13*(2), Article 021039. https://doi.org/10.1103/PhysRevX.13.021039

Krämer, S., Plankensteiner, D., Ostermann, L., & Ritsch, H. (2018). QuantumOptics.jl: A Julia framework for simulating open quantum systems. *Computer Physics Communications*, *227*, 109–116. https://doi.org/10.1016/j.cpc.2018.02.004

Le Jeannic, H., Ramos, T., Simonsen, S. F., Pregnolato, T., Liu, Z., Schott, R., Wieck, A. D., Ludwig, A., Rotenberg, N., García-Ripoll, J. J., & Lodahl, P. (2021). Experimental reconstruction of the few-photon nonlinear scattering matrix from a single quantum dot in a nanophotonic waveguide. *Physical Review Letters*, *126*(2), Article 023603. https://doi.org/10.1103/PhysRevLett.126.023603

Lodahl, P., Mahmoodian, S., Stobbe, S., Rauschenbeutel, A., Schneeweiss, P., Volz, J., Pichler, H., & Zoller, P. (2017). Chiral quantum optics. *Nature*, *541*(7638), 473–480. https://doi.org/10.1038/nature21037

Mahmoodian, S., Čepulkovskis, M., Das, S., Lodahl, P., Hammerer, K., & Sørensen, A. S. (2018). Strongly correlated photon transport in waveguide quantum electrodynamics with weakly coupled emitters. *Physical Review Letters*, *121*(14), Article 143601. https://doi.org/10.1103/PhysRevLett.121.143601

Mahmoodian, S., Lodahl, P., & Sørensen, A. S. (2016). Quantum networks with chiral-light-matter interaction in waveguides. *Physical Review Letters*, *117*(24), Article 240501. https://doi.org/10.1103/PhysRevLett.117.240501

Miao, Q., & Agarwal, G. S. (2025). Transparency, nonclassicality, and nonreciprocity in chiral waveguide quantum electrodynamics. *Physical Review Research*, *7*(1), Article 013138. https://doi.org/10.1103/PhysRevResearch.7.013138

Mitsch, R., Sayrin, C., Albrecht, B., Schneeweiss, P., & Rauschenbeutel, A. (2014). Quantum state-controlled directional spontaneous emission of photons into a nanophotonic waveguide. *Nature Communications*, *5*, Article 5713. https://doi.org/10.1038/ncomms6713

Pennetta, R., Blaha, M., Johnson, A., Lechner, D., Schneeweiss, P., Volz, J., & Rauschenbeutel, A. (2022). Collective radiative dynamics of an ensemble of cold atoms coupled to an optical waveguide. *Physical Review Letters*, *128*(7), Article 073601. https://doi.org/10.1103/PhysRevLett.128.073601

Pennetta, R., Lechner, D., Blaha, M., Rauschenbeutel, A., Schneeweiss, P., & Volz, J. (2022). Observation of coherent coupling between super- and subradiant states of an ensemble of cold atoms collectively coupled to a single propagating optical mode. *Physical Review Letters*, *128*(20), Article 203601. https://doi.org/10.1103/PhysRevLett.128.203601

Pichler, H., Ramos, T., Daley, A. J., & Zoller, P. (2015). Quantum optics of chiral spin networks. *Physical Review A*, *91*(4), Article 042116. https://doi.org/10.1103/PhysRevA.91.042116

Rosiński, J., Gawełczyk, M., Tarnowski, K., Karwat, P., Wigger, D., & Machnikowski, P. (2024). Quantum dots as optimized chiral emitters for photonic integrated circuits. *Physical Review B*, *109*(8), Article 085431. https://doi.org/10.1103/PhysRevB.109.085431

Sheremet, A. S., Petrov, M. I., Iorsh, I. V., Poshakinskiy, A. V., & Poddubny, A. N. (2023). Waveguide quantum electrodynamics: Collective radiance and photon-photon correlations. *Reviews of Modern Physics*, *95*(1), Article 015002. https://doi.org/10.1103/RevModPhys.95.015002

Solano, P., Barberis-Blostein, P., & Sinha, K. (2023). Dissimilar collective decay and directional emission from two quantum emitters. *Physical Review A*, *107*(2), Article 023723. https://doi.org/10.1103/PhysRevA.107.023723

Söllner, I., Mahmoodian, S., Hansen, S. L., Midolo, L., Javadi, A., Kiršanske, G., Pregnolato, T., El-Ella, H., Lee, E. H., Song, J. D., Stobbe, S., & Lodahl, P. (2015). Deterministic photon-emitter coupling in chiral photonic circuits. *Nature Nanotechnology*, *10*(9), 775–778. https://doi.org/10.1038/nnano.2015.159

Yao, X., & Li, P. (2025). Tunable directional collective emission of two or three quantum emitters in a chiral waveguide. *Optics Express*, *33*(13), 28437. https://doi.org/10.1364/OE.567080